Chemical Science

ROYAL SOCIETY OF CHEMISTRY

EDGE ARTICLE

View Article Online
View Journal | View Issue

Cite this: *Chem. Sci.*, 2024, **15**, 5376

All publication charges for this article have been paid for by the Royal Society of Chemistry

Received 10th January 2024
Accepted 29th February 2024

DOI: 10.1039/d4sc00201f

rsc.li/chemical-science

Sequential radical and cationic reactivity at separated sites within one molecule in solution†

Shihua Liu,‡[a] Yinwu Li,‡[b] Jieli Lin,[a] Zhuofeng Ke,[b] Hansjörg Grützmacher,[ac] Cheng-Yong Su[a] and Zhongshu Li*[a]

Distonic radical cations (DRCs) with spatially separated charge and radical sites are expected to show both radical and cationic reactivity at different sites within one molecule. However, such "dual" reactivity has rarely been observed in the condensed phase. Herein we report the isolation of crystalline $1\lambda^2,3\lambda^2$-1-phosphonia-3-phosphinyl-cyclohex-4-enes **2a,b**$^{\bullet+}$, which can be considered delocalized DRCs and were completely characterized by crystallographic, spectroscopic, and computational methods. These DRCs contain a radical and cationic site with seven and six valence electrons, respectively, which are both stabilized *via* conjugation, yet remain spatially separated. They exhibit reactivity that differs from that of conventional radical cations (CRCs); specifically they show sequential radical and cationic reactivity at separated sites within one molecule in solution.

Introduction

Stable organic radicals, such as the triphenylmethyl radical, already discovered in 1900,[1] or Thiele's hydrocarbon – the first well-characterized hydrocarbon diradicaloid discovered shortly thereafter,[2] have found numerous applications ranging from synthetic chemistry to materials sciences.[3] In classical radical cations, the charge and spin density are localized on one atom or delocalized across a group of atoms. These radicals are classified as conventional radical cations (CRCs). The octet rule predicts that a neutral radical $R_3E^{\bullet}$, or cationic radical $R_3E^{\bullet+}$ with seven valence electrons will react with a second radical $R_1^{\bullet}$, under the formation of a shared two electron bond to give neutral $R_3E–R_1$ or cationic $[R_3E–R_1]^{+\bullet}$.[4] The same holds true when a six-valence electron cation R_3E^+ reacts with a nucleophile Nu^- as a two electron donor. In contrast, a reaction between a CRC and Nu^- will result in a high-energy radical with nine valence electrons, which is difficult to achieve when E is an element from the second and/or third period (Fig. 1a).

Distonic radical cations (DRCs) are a special class of radical cations with spatially separated charge and radical sites.[5] A large number of DRCs have been studied in the gas phase,[6] and

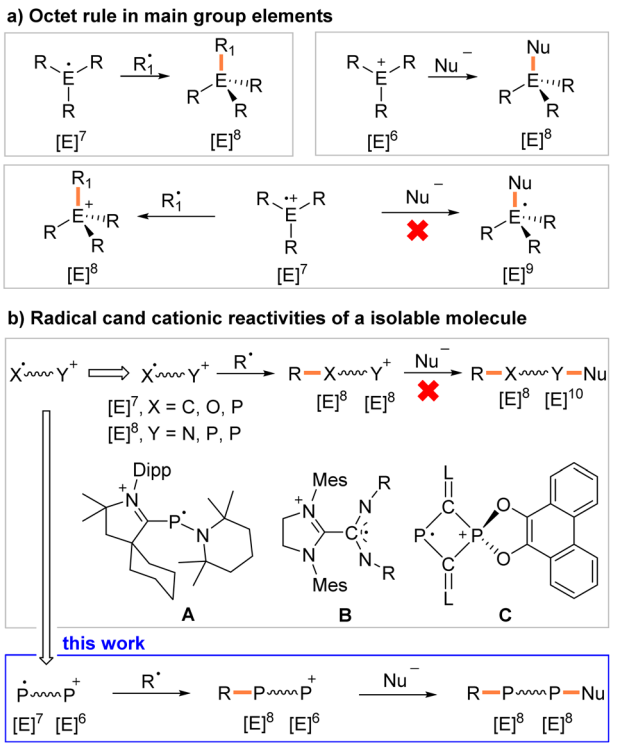

Fig. 1 Octet rule in controlling the reactivity of (a) neutral radicals, cations, and conventional radical cations, and (b) distonic radical cations. Dipp, 2,6-diisopropylphenyl; Mes, 2,4,6-trimethylphenyl; L, 1,3-bis(2,6-diisopropylphenyl)imidazoline-2-ylidene.

[a]*LIFM, IGCME, School of Chemistry, Sun Yat-Sen University, Guangzhou 510006, China. E-mail: lizhsh6@mail.sysu.edu.cn*

[b]*School of Materials Science and Engineering, Sun Yat-Sen University, 510006 Guangzhou, China*

[c]*Department of Chemistry and Applied Biosciences, ETH Zürich, Vladimir-Prelog-Weg 1, Zürich 8093, Switzerland*

† Electronic supplementary information (ESI) available: Synthesis and characterization of compounds, NMR spectra, and crystallographic and computational details. CCDC 2215136–2215138, 2215140–2215143 and 2314776. For ESI and crystallographic data in CIF or other electronic format see DOI: https://doi.org/10.1039/d4sc00201f

‡ These authors contributed equally to this work.

so called "dual reactivity" has been observed with distonic acylium radicals. Specifically, radical coupling reactivity at the radical site and cycloaddition reactivity at the acylium cation site were demonstrated.[7] But most DRCs are fleeting reactive intermediates in solution,[8] or in crystalline or rigid matrices,[9] and only a very limited number of crystallographically characterized DRCs are known.[10] The group of Bertrand (**A**, Fig. 1b), Wang, and Schulz independently disclosed DRCs with a cationic carbene moiety and a radical center localized mainly on a phosphorus atom.[10a,b,e] Johnson reported a DRC with again a cationic imidazolium unit and a radical site delocalized over a carbodiimide moiety (**B**, Fig. 1b).[10c] Recently, we described the heterocyclic DRC **C** (Fig. 1b) with a two-coordinated radical λ^2,σ^2-P-center and four-coordinated cationic λ^4,σ^5-P-phosphonium center within a central C_2P_2 ring.[10f] But these DRCs show only radical reactivity.[10a,e,f]

To the best of our knowledge, dual reactivity within one molecule, including CRCs, DRCs, and charged nitroxide radicals,[11] has not been reported in the condensed phase.[12] We report here the synthesis and characterization of crystalline, room-temperature (RT) stable $1\lambda^2,3\lambda^2$-1-phosphonia-3-phosphinyl-cyclohex-4-enes **2a,b**$^{\bullet+}$(BAr^F) (BAr^F = [B(3,5-(CF$_3$)$_2$C$_6$H$_3$)$_4$]$^-$). They contain formally a neutral two-coordinated phosphanyl P(II) radical site with seven and a two-coordinated phosphenium P(III) cation center with six valence electrons (Scheme 1). Hence both sites are electronically and coordinatively unsaturated. These features allow the study of the unique sequential radical and cationic reactivity at separated sites within one molecule (Fig. 1b).

Results and discussion

Synthesis of DRCs 2a,b$^{\bullet+}$

We recently reported the reaction of imidazolium-stabilized diphosphete-diide **IDP** (ref. 13) with one equivalent of a phosphaalkyne yielding tricyclic neutral L$_2$(Ph$_3$C)C$_3$P$_3$ derivatives (L = **IPr** = 1,3-bis(2,6-diisopropylphenyl)imidazolium-2-ylidene), which upon oxidation rearranged cleanly into a radical cation [L$_2$(Ph$_3$C)C$_3$P$_3$]$^{\bullet+}$ with an almost planar C$_3$P$_3$ cycle over which the spin density is more or less evenly delocalized.[14] We now reacted **IDP** with alkynes, such as *tert*-butyl phenylpropiolate (PTP) or diethyl acetylenedicarboxylate,[15] which led to yellow powders **1a,b** in 90–95% yield, respectively (Scheme 1). Multinuclear NMR spectroscopy and single-crystal X-ray diffraction analyses unambiguously identify these compounds as [2 + 2] cycloaddition products [(L)$_2$C$_2$P$_2$C(R$_1$)C(R$_2$)] (**1a,b**, L = **SIPr** = 1,3-bis(2,6-diisopropylphenyl)imidazoline-2-ylidene). Monitoring the reaction process by ^{31}P NMR spectroscopy indicated the formation of **1a** as a sole new product with the appearance of two doublets at 158.8 and 153.8 ppm ($^2J_{PP}$ = 6.5 Hz). The solid-state structure of **1a**, obtained by X-ray diffraction (XRD) methods using single crystals, confirms the [2.1.1] bicyclic skeleton (Fig. 1a). The synthesis and characterization of **1b** were reported by us.[15] Similar reactivity between (RN)$_2$P$_2$ biradicaloids and alkynes has been observed previously by Schulz *et al.*[16]

No decomposition or rearrangement was observed after heating toluene solutions of **1a,b** at 100 °C for more than 4 hours. The cyclic voltammogram of **1a**, selected as an example, shows an irreversible one electron oxidation at E_P = +0.07 V *vs.* Fc$^+$/Fc (Fig. 2b). Adding 0.8 equivalent of the ferrocenium salt Fc$^+$(BAr^F), dissolved in diethyl ether to a diethyl ether solution of **1a,b** at −30 °C, led to highly air sensitive, paramagnetic, green compounds **2a,b**$^{\bullet+}$(BAr^F) in high yield (Scheme 1). Excess Fc$^+$(BAr^F) was found to react further with **2a,b**$^{\bullet+}$(BAr^F). Of note, the reactions between **IDP** and diphenylacetylene or methyl(phenyl)acetylene also gave the expected cycloaddition products but they show no clean redox chemistry. XRD methods and EPR spectroscopy confirm the structure of these compounds as $1\lambda^2,3\lambda^2$-1-phosphonia-3-phosphinyl-cyclohex-4-ene radical cation salts **2a,b**$^{\bullet+}$(BAr^F) (Scheme 1). Note that no apparent decomposition was observed after heating the tetrahydrofuran solution of **2a,b**$^{\bullet+}$(BAr^F) at 60 °C for more than 48 hours, and the reaction of the stable radical cation IDP$^{\bullet+}$(BAr^F)[13] with alkynes does not allow the synthesis of **2a,b**$^{\bullet+}$(BAr^F).

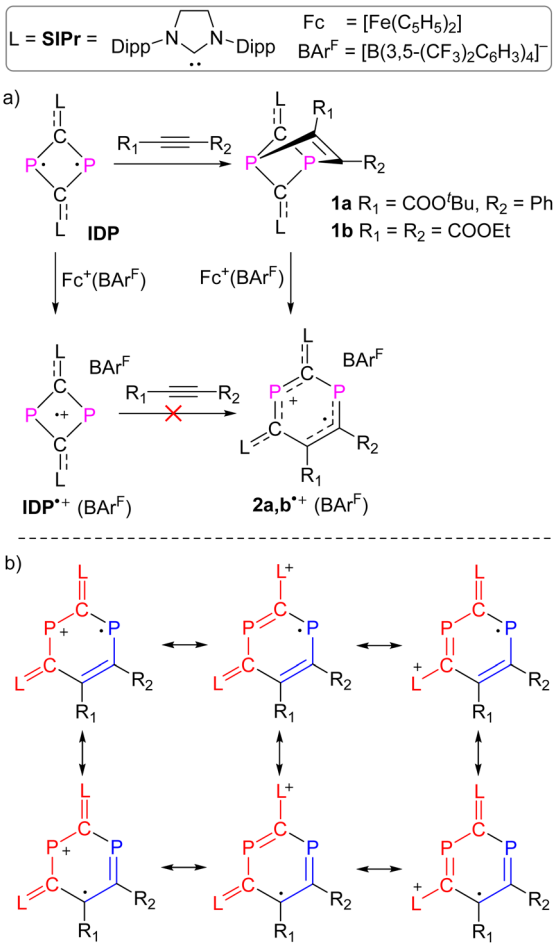

Scheme 1 (a) Synthesis of compounds **1** and **2**$^{\bullet+}$(BAr^F); (b) selected resonance structures of DRC **2**$^{\bullet+}$ in order to indicate delocalization of the positive charge in the red part of the molecule and delocalization of the spin in the blue area.

Characterization of DRCs 2a,b$^{\bullet+}$

The EPR spectra at RT show a doublet of doublets due to a large and a very small isotropic ^{31}P hyperfine coupling constant

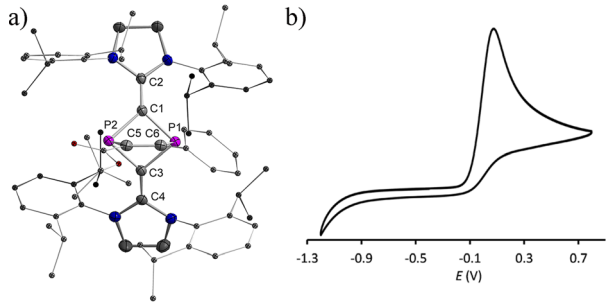

Fig. 2 (a) Plots of the molecular structure of **1a** (ellipsoids are set to 50% probability; H atoms and solvents are omitted for clarity). Selected distances (Å): P1–C1 1.838(2), P1–C3 1.838(2), C3–P2 1.850(2), P2–C1 1.843(2), C1–C2 1.352(3), C3–C4 1.349(3), P1–C6 1.917(2), P2–C5 1.900(2), and C5–C6 1.353(3); (b) cyclic voltammogram for 10^{-3} M THF solution of **1a** containing 0.1 M *n*-$Bu_4N(BAr^F)$ as electrolyte (potential *versus* Fc^+/Fc) at scan rate 100 mV s^{-1} with platinum as the working and counter electrode and Ag/Ag^+ as the reference electrode.

(HFC) (av. $a_{iso}(P1) = 108.0$ MHz and $a_{iso}(P2) = 11.5$ MHz) for $\mathbf{2a}^{\bullet+}(BAr^F)$ (Fig. 3a). For $\mathbf{2b}^{\bullet+}(BAr^F)$, only a doublet is observed due to a large isotropic ^{31}P hyperfine interaction [av. $a_{iso}(P1) = 85.7$ MHz and $g_{iso} = 2.008$] (Fig. S24†). The HFC with the P1 nucleus is smaller than the ones observed for comparable phosphorus centered radicals where the spin is predominantly localized on the P center (spin density > 0.5*e*, a_{iso} > 150 MHz).[10a,b,13,17] This indicates delocalization of the spin density but very little is localized on P2. In frozen solution at 100 K, a strongly anisotropic EPR spectrum is recorded (Fig. 3b). The simulation of the spectrum yielded the principal *g* values and ^{31}P HFCs for $\mathbf{2a}^{\bullet+}(BAr^F)$ ($g = [2.0042, 2.0091, 2.0130]$, $A(^{31}P1) = [-23.1, 5.05, 342.1]$ MHz, $A(^{31}P2) = [-25.3, 10.6, 49.2]$ MHz). The large anisotropic ^{31}P HFC tensor confirms that the majority of spin density is indeed localized in a p-type orbital at P1 (Fig. 3c). The EPR spectrum of the frozen solution of $\mathbf{2b}^{\bullet+}(BAr^F)$ is too broad to be simulated (Fig. S25†).

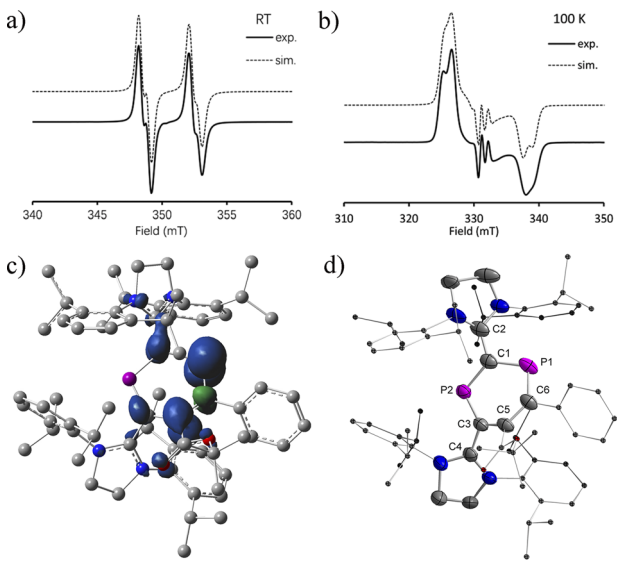

Fig. 3 (a) Continuous wave EPR spectra at RT and (b) at 100 K; (c) calculated spin density (density = 0.004); and (d) plots of the molecular structure of $\mathbf{2a}^{\bullet+}(BAr^F)$ (ellipsoids are set to 50% probability; H atoms and anions are omitted for clarity). Selected distances (Å): $\mathbf{2a}^{\bullet+}$: P1–C1 1.785(5), P1–C6 1.725(5), C6–C5 1.412(6), C5–C3 1.455(6), C3–P2 1.719(4), P2–C1 1.735(4), C1–C2 1.444(6), and C3–C4 1.470(5).

Slow evaporation of a saturated diethyl ether/hexane solution (1 : 1) at RT yielded green single crystals of $\mathbf{2a,b}^{\bullet+}(BAr^F)$ suitable for X-ray diffraction studies. Both compounds have very similar structures with a central six-membered C_4P_2 heterocycle with two λ^2-phosphorus atoms in the 1,3-position as a result of a skeletal rearrangement (Fig. 3d and S24†). The exocyclic C–L bonds in $\mathbf{2a}^{\bullet+}$ (av. 1.457 Å) and in $\mathbf{2b}^{\bullet+}$ (av. 1.452 Å) are longer than those of **1a** (av. 1.351 Å) and **1b** (av. 1.356 Å),[15] but rather similar to the ones observed in $\mathbf{IDP}^{\bullet+}$ (av. 1.41 Å), indicating a strong electron-donation from the **SIPr** to the C_4P_2 heterocycle but little back-donation.[3a,c,18] On one hand, the lengths of the P1–C6 (av. 1.736 Å) and C6–C5 (av. 1.393 Å) bonds in $\mathbf{2a,b}^{\bullet+}$ indicate a conjugated P1–C6–C5 unit over which the unpaired electrons are mainly delocalized. On the other hand, the P2–C1 (av. 1.751 Å) and P2–C3 (av. 1.722 Å) bonds are within the range observed in cyclic phosphenium cations (1.716–1.763 Å) and indicate delocalization of the positive charge in these units.[17b,19] Both the P1–C6–C5 and C1–P2–C3 parts are connected *via* P1–C1 (av. 1.789 Å) and C3–C5 (av. 1.457), which are significantly longer. These structure parameters, in conjunction with the EPR analyses and theoretical calculations (*vide infra*), are in accord with the resonance structures shown in Scheme 1b, which indicate that the spin is mainly delocalized in the blue part and the positive charge is mainly in the red part of the molecule. Both halves are connected by elongated P1–C1 and C3–C5 bonds, respectively.

The molecular structures of $\mathbf{2a,b}^{\bullet+}$ were further examined using density functional theory (DFT) calculations optimized at the level of (U)M06-2X/def2-SVP[20] and natural bond orbital (NBO) analysis at the level of (U)M06-2X/def2-TZVP.[21] The composition of molecular orbitals (MOs) and natural localized MOs (NLMOs) evolving from an NBO analysis supports the description of $\mathbf{2a,b}^{\bullet+}$ as DRCs (Fig. 4 and S26†). In the case of $\mathbf{2a}^{\bullet+}$, MO analysis revealed no apparent difference between the α-LUMO and β-LUMO+1 and between α-SOMO and β-LUMO, where the former two empty MOs comprise mainly a π-type lone pair at P2 with contributions from adjacent π-type bonding orbitals of the CL fragments (CL = C-SIPr, Fig. 4a). The latter involves mainly singly occupied and empty allyl-type MOs with a small contribution from adjacent π-type bonding orbitals of the CL fragments (Fig. 4b). These results imply the partial separation of charge and spin density in $\mathbf{2a}^{\bullet+}$. The NLMOs disclose an α-electron at the π-type bonding orbital on P1(65%)–C6(31%), an α-electron delocalized over P1(6%)–C6(13%)–C5(68%), and an β-electron at the π-type bonding orbital P1(9%)–C6(51%)–C5(32%). These results indicate the presence of a delocalized allyl-type endocyclic P1–C6═C5 radical fragment where two α-electrons and one β-electron are delocalized over the π-type bonding orbital. Natural population analysis (NPA) reveals that the spin density in $\mathbf{2a}^{\bullet+}$ is localized mainly at P1 (0.41*e*), C6 (−0.11*e*), and C5 (0.30*e*), with very small contributions from C1 (0.10*e*) and C3 (0.07*e*), and virtually no

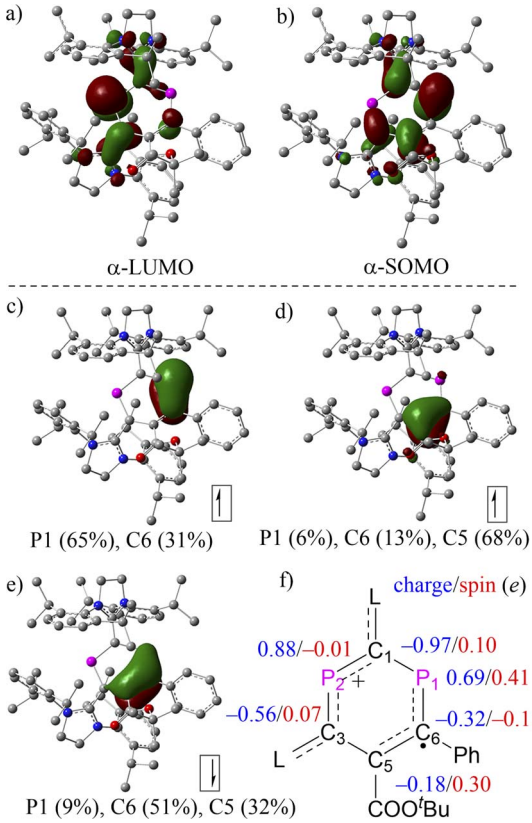

Fig. 4 Selected (a) α-LUMO; (b) β-SOMO, and NLMOs resulting from an NBO analysis of **2a**$^{\bullet+}$: (c) a π-bond α-electron; (d) a π-bond α-electron; (e) a π-bond β-electron; (f) selected NPA charges and spin populations.

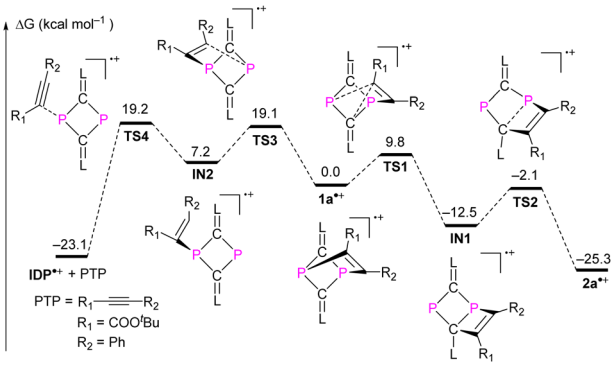

Fig. 5 Free energy profile for the formation of **2a**$^{\bullet+}$ or **IDP**$^{\bullet+}$ and PTP from the transient radical cation intermediate **2a**$^{\bullet+}$.

spin density on P2 (−0.01*e*), which agrees with the analysis of EPR spectra. Additional spin density is delocalized over CL fragments (Fig. 3c). In addition, the P2 center within the phosphenium unit carries the highest positive charge (**2a**$^{\bullet+}$: +0.69*e* for P1 and +0.88*e* for P2). An inspection of the Wiberg bond indices (WBIs) shows that the P1–C1 (1.00) and C5–C3 (1.13) connecting the two subunits P1–C6–C5 and C1–P2–C3 are nearly single bonds, and their bond orders are substantially smaller than the rest of the endocyclic bonds, such as P1–C6 (1.26), C6–C5 (1.40), C3–P2 (1.35), and P2–C1 (1.17). The WBIs of bonds linking the P2C4 cycle to the L substituents, C1–C2 (1.22) and C3–C4 (1.11), further support the strong electron-donation from **SIPr**. The presence of the two carboxylic ester units COOEt as stronger electron-withdrawing substituents renders the two phosphorus centers (+0.75*e* for P1 and +0.90*e* for P2) in **2b**$^{\bullet+}$ slightly more positively charged than those in **2a**$^{\bullet+}$, but otherwise the electronic structures of **2a**$^{\bullet+}$ and **2b**$^{\bullet+}$ are very similar (Fig. S26†).

Possible mechanism for the formation of DRCs 2$^{\bullet+}$

The mechanism leading to **2a**$^{\bullet+}$ from the putative intermediate radical cation **1a**$^{\bullet+}$ – as a product of the one-electron oxidation of **1a** – was investigated using DFT calculations ((U)SMD-M06-2X/def2-TZVP//(U)M06-2X/def2-SVP) for **2a**$^{\bullet+}$ as a selected example. A possible minimum energy reaction pathway (MERP) is shown in Fig. 5.[20] The intramolecular rearrangement starts from the [2.1.1] bicyclic radical cation **1a**$^{\bullet+}$, which is at ΔG = 0.0 kcal mol^{-1} on the relative energy scale. The 1,2-shift of the CR_1 group from a P center to the adjacent carbon center of the CL unit only requires 9.8 kcal mol^{-1} to reach the activated complex at **TS1**. Intermediate **IN1** is formed in an exergonic reaction (ΔG = −12.5 kcal mol^{-1}). This further rearranges again *via* an activated complex at an energetically low-lying transition state **TS2** (10.4 kcal mol^{-1}) to give the six-membered DRC **2a**$^{\bullet+}$ in an exergonic reaction (−12.8 kcal mol^{-1}). We also investigated the alkyne dissociation from **2a**$^{\bullet+}$, which is the microscopically reverse reaction of the addition of an alkyne to the radical cation **IDP**$^{\bullet+}$. As the left branch of the MERP shows, this dissociation is indeed a thermodynamically preferred process (ΔG = −23.1 kcal mol^{-1}) but requires the formation of activated complexes at energetically higher lying transition states **TS3** (19.1 kcal mol^{-1}) and **TS4** (19.2 kcal mol^{-1}), respectively, which disfavours this process kinetically. Thus, the calculations are in good agreement with the experimental results, which show that (i) one-electron oxidation of **1a** exclusively leads to **2a**$^{\bullet+}$ and (ii) that the reaction between **IDP**$^{\bullet+}$ and PTP will not give **2a**$^{\bullet+}$.

Treatment of **2a**$^{\bullet+}$(BAr^F) with an excess of Mg powder as a reducing agent at RT under vigorous stirring overnight did not regenerate the neutral tricyclic species **1a**, but yielded a red powder **3** with excellent yield 91% (Scheme 2). Attempts to reduce **2b**$^{\bullet+}$(BAr^F) under the same reaction conditions led to a mixture of unidentified products. The ^{31}P spectrum of **3** shows two doublets at −154.1 ppm and −197.1 ppm ($^1J_{PP}$ = 64.8 Hz), which is in the range of diphosphiranes (−117 – −176 ppm).[22] Indeed, XRD analysis of a single crystal of **3** unambiguously confirms the formation of a [3.1.0] bicyclic skeleton and a CP_2

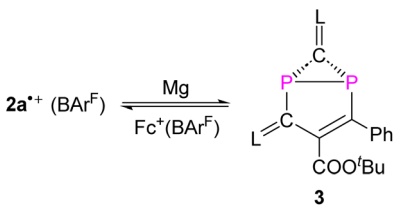

Scheme 2 Synthesis of compound **3**.

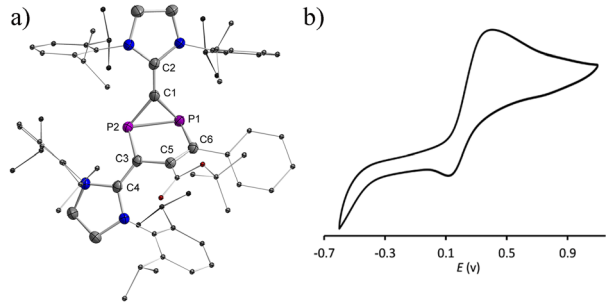

Fig. 6 (a) Plots of the molecular structure of **3** (ellipsoids are set to 50% probability; H atoms and solvents are omitted for clarity). Selected distances (Å): P1–P2 2.2685(6), P1–C1 1.8075(19), P1–C6 1.8408(17), C6–C5 1.376(2), C5–C3 1.468(2), C3–P2 1.8387(17), P2–C1 1.7911(19), C1–C2 1.365(3), and C3–C4 1.383(2); (b) cyclic voltammogram for 10^{-3} M THF solution of **3** containing 0.1 M *n*-$Bu_4N(BAr^F)$ as electrolyte (potential *versus* Fc^+/Fc) at scan rate 100 mVs^{-1} with platinum as the working and counter electrode and Ag/Ag^+ as the reference electrode.

phosphirane ring annealed to an unsaturated five-membered C_3P_2 ring (Fig. 6a). The P1–P2 bond [2.2685(6) Å] is slightly longer than standard P–P single bonds (2.214 Å *vs.* 3.124 Å in $\mathbf{2a}^{\bullet+}$)[23] and comparable with the P–P bonds (2.167–2.223 Å) in similar housane-type NP_2 fragment reported by the group of Schulz.[16a,b,24] The P–C bonds in the phosphirane moiety [P1–C1 1.8075(19); P2–C1 1.7911(19) Å] are notably shorter than the ones in the five-membered C_3P_2 ring [P1–C6 1.8408(17); P2–C1 1.7911(19) Å]. The C5=C6 bond [1.376(2) Å] corresponds to a double bond, while the adjacent C5–C3 bond [1.468(2) Å] is significantly longer. The fold angle between the three- and five-membered rings amounts to 100°. The cyclic voltammogram of **3** shows a quasi-reversible redox wave at $E_P = +0.42$ V *vs.* Fc^+/Fc (Fig. 6b). Indeed, one-electron oxidation of **3** with $Fc^+(BAr^F)$ led cleanly to $\mathbf{2a}^{\bullet+}(BAr^F)$ suggesting that the conversion $\mathbf{2a}^{\bullet+} + e \leftrightarrows \mathbf{3}$ is fully reversible.

Note that the reaction of **IDP** with trityl phosphaalkyne resulted in a bicyclic product similar to that of **3** (Scheme 2), and the subsequent one electron oxidation afforded a delocalized cyclic C_3P_3 radical cation instead of a DRC.[14] Wang and co-workers recently demonstrated that electron-withdrawing groups in indeno[2,1-*b*]fluorenes favor a triplet ground state over a singlet ground state.[25] This observation suggests that electron-withdrawing groups can impede electron delocalization to some extent and we therefore assume that the DRC character of $\mathbf{2a,b}^{\bullet+}$ is caused by the carboxylate residues as electron withdrawing groups.

Reactivity of DRCs $\mathbf{2a,b}^{\bullet+}$

To probe chemically the sequential radical and cationic reactivity of $\mathbf{2a,b}^{\bullet+}$ as delocalized DRCs, $\mathbf{2a}^{\bullet+}(BAr^F)$ was selected to react with half an equivalent of diphenyl disulfide. The reaction between phosphorus radicals and disulfides to give compounds with a P–S bond is well documented,[10f,15,26] and we expected that the radical center P1 would add to PhS$^\bullet$ to give product $\mathbf{4}^+(BAr^F)$ as an EPR silent but an NMR active product. This is indeed the case and $\mathbf{4}^+(BAr^F)$ is obtained as red powder in 90% yield

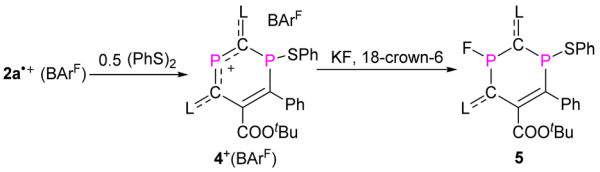

Scheme 3 Synthesis of compounds $\mathbf{4}^+(BAr^F)$ and **5**.

(Scheme 3). The ^{31}P NMR spectrum of $\mathbf{4}^+(BAr^F)$ displays resonance signals at 309.2 ppm for the two-coordinated phosphenium center P2 and at 6.3 ppm for the three-coordinated λ^3, σ^3-P1 nucleus. The solid-state structure of $\mathbf{4}^+(BAr^F)$ is shown in Fig. 7a. The formation of a new P1–S1 bond [2.2123(16) Å; $\sum r_{cov}(P\text{–}S) = 2.14$ Å][23] interrupts the electron delocalization mainly within the endocyclic P1–C6–C5 skeleton where the spin was delocalized in $\mathbf{2a}^{\bullet+}$. For instance, a significantly shortened C5=C6 bond [1.363(4) Å, *vs.* 1.412(6) Å in $\mathbf{2a}^{\bullet+}$] and elongated P1–C6 bond [1.818(3) Å, *vs.* 1.725(5) Å in $\mathbf{2a}^{\bullet+}$] are observed. Other structural changes are noticeable but smaller. On the other side, the C4–C3–P2–C1–C2 unit in $\mathbf{4}^+$ has similar structural parameters to the one observed in the $\mathbf{2a}^{\bullet+}$ underlining that this part is still best described as a delocalized phosphenium cation (Table S2†).

The cation $\mathbf{4}^+$ reacted cleanly with fluoride, but did not react with other halogen anions, azide, or cyanate. The treatment of $\mathbf{4}^+(BAr^F)$ with three equivalents of potassium fluoride in the presence of equimolar 18-crown-6 gave a yellow powder **5** in 73% yield (Scheme 3). In the ^{31}P NMR spectrum, **5** shows only one doublet at 146.7 ppm ($^1J_{PF} = 918.1$ Hz) and one singlet at 13.5 ppm, while in the ^{19}F NMR spectrum, one major isomer at −124.2 ppm ($^1J_{PF} = 919.3$ Hz) and a second minor isomer at −127.6 ppm ($^1J_{PF} = 926.4$ Hz) were observed. This agrees well with the result from an XRD study (Fig. 7b), which shows two isomers, which co-crystallized in one single crystal with a major *trans*-isomer [P2–F1 1.622(2) Å, 78%] and a *cis*-isomer (P2–F1A 1.574(6) Å, 22%) (*trans*- and *cis*-indicate the mutual position of the P–F and P–S bonds with respect to the ring plane). There is rather little structural change between $\mathbf{4}^+$ and **5** and only the P2–C1 [1.801(3) Å] and P2–C3 [1.798(3) Å] bonds in **5** are evidently elongated.

Finally, the reactivity of $\mathbf{2a,b}^{\bullet+}$ toward various nucleophiles was probed. The reactions of $\mathbf{2a,b}^{\bullet+}(BAr^F)$ with KF, CsF, Et_3NHF, potassium triethylborohydride, phenylmagnesium chloride, 1,3,4,5-tetramethylimidazol-2-ylidene or 4-dimethylaminopyridine afforded mixtures of compounds, which are NMR active but remained unidentified. Treatment of $\mathbf{2a}^{\bullet+}(BAr^F)$ with excess sodium azide (NaN_3) afforded mainly compound $\mathbf{6}^+(BAr^F)$ along with minor amounts of **3** and other unidentified products (Scheme 4 and Fig. S21†). Recrystallization of the crude product led to 15% yield of crystalline reddish materials of $\mathbf{6}^+(BAr^F)$, which are still contaminated with minor impurities. We assume that the formation of $\mathbf{6}^+(BAr^F)$ is the result of the reaction of $\mathbf{2a}^{\bullet+}(BAr^F)$ with a transient azidyl radical ($N_3^\bullet$), which is generated *via* the oxidation of N_3^- by $\mathbf{2a}^{\bullet+}(BAr^F)$. Single electron reduction of $\mathbf{2a}^{\bullet+}(BAr^F)$ would lead to **3** in accordance with its observation. Note, in this context, that the generation of $N_3^\bullet$ by

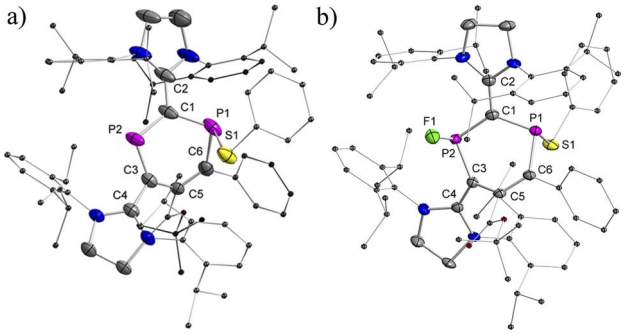

Fig. 7 Plots of the molecular structures of $4^{+}(BAr^{F})$ and **5** (ellipsoids are set to 50% probability; H atoms, anions, and solvents are omitted for clarity). Selected distances (Å): (a) 4^{+}: P1–S1 2.2123(16), P1–C1 1.808(4), P1–C6 1.818(3), C6–C5 1.363(4), C5–C3 1.487(4), C3–P2 1.723(3), P2–C1 1.752(3), C1–C2 1.432(5), and C3–C4 1.473(4); (b) **5** (only the *trans*-isomer of **5** is shown): P1–S1 2.1241(10), P1–C1 1.798(3), P1–C6 1.825(3), C6–C5 1.361(4), C5–C3 1.489(3), C3–P2 1.798(3), P2–C1 1.801(3), P2–F1 1.622(2), C1–C2 1.393(4), and C3–C4 1.395(3).

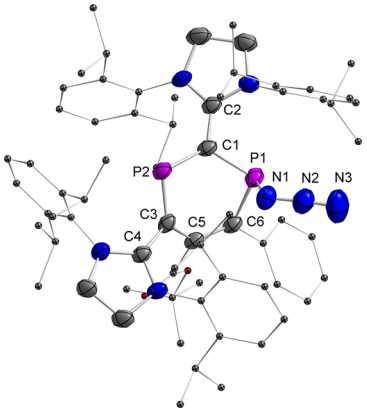

Fig. 8 Plots of the molecular structure of $6^{+}(BAr^{F})$ (ellipsoids are set to 50% probability; H atoms, anions, and solvents are omitted for clarity). Selected distances (Å): 6^{+}: P1–N1 1.775(3), N1–N2 1.215(5), N2–N3 1.142(6), P1–C1 1.794(3), P1–C6 1.814(4), C6–C5 1.359(5), C5–C3 1.483(4), C3–P2 1.723(4), P2–C1 1.746(4), C1–C2 1.415(5), and C3–C4 1.470(5).

electrochemical or chemical oxidation of azide with 2,2,6,6-tetramethyl-1-oxopiperidinium ($TEMPO^{+}$) has been studied extensively in synthetic chemistry.[27] In the ^{31}P NMR spectra, singlets at 305.7 and 42.7 ppm for $6^{+}(BAr^{F})$ were observed. And XRD studies confirmed the molecular structure of $6^{+}(BAr^{F})$ (Fig. 8). The azidyl group is bound to the radical site P1 leaving the cationic P2 site unreacted. The newly formed P1–N1 bond [1.775(3) Å] corresponds to a single bond. The other structural parameters of $6^{+}(BAr^{F})$ are comparable to the ones observed in $4^{+}(BAr^{F})$.

Treatment of $2b^{\bullet+}(BAr^{F})$ with one equivalent of (trimethylsilyl)diazomethane at RT led to a spontaneous colour change from green to blue. After stirring the solution for 1 hour, we observed the formation of an EPR active paramagnetic species $7^{\bullet+}(BAr^{F})$ resulting from a [2 + 1] cycloaddition reaction under the elimination of dinitrogen (Scheme 4). The EPR spectra of diethyl ether solutions of $7^{\bullet+}(BAr^{F})$ at RT and 100 K show HFC tensors to which clearly only one ^{31}P nucleus contributes with a relatively large ^{31}P hyperfine interaction g = [2.0041, 2.0165, 2.0081], g_{iso} = 2.010, $A(^{31}P1)$ = [−1.9, −2.8, 317.7] Mz, and $a_{iso}(P1)$ = 104.4 MHz (Fig. 9a and b), which is comparable with that of $2a,b^{\bullet+}(BAr^{F})$. The solid-state structure of $7^{\bullet+}(BAr^{F})$ is shown in Fig. 9d. The fold angle between the three-membered C_2P and six-membered C_4P_2 ring within the [4.1.0] bicyclic skeleton is 104°. The P1–C6 (1.867(2) Å), P1–C7 (1.848(2) Å), and C6–C7 (1.532(3) Å) bonds in the phosphirane ring are in the range of classical single bonds ($\sum r_{cov}$(P–C) = 1.86 Å, $\sum r_{cov}$(P=C) = 1.69 Å, $\sum r_{cov}$(C–C) = 1.50 Å, and $\sum r_{cov}$(C=C) = 1.34 Å).[23] A new double bond is established between C3=C5 (1.381(3) Å) while the adjacent C5–C6 bond is elongated to 1.487(3) Å [*vs.* C5–C6 1.373(3) Å in $2b^{\bullet+}$, Fig. S27†].

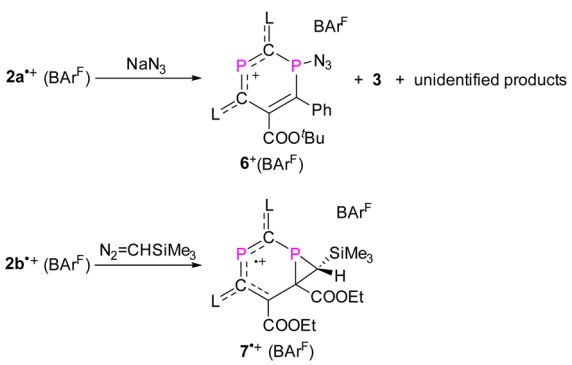

Scheme 4 Synthesis of compounds $6^{+}(BAr^{F})$ and $7^{\bullet+}(BAr^{F})$.

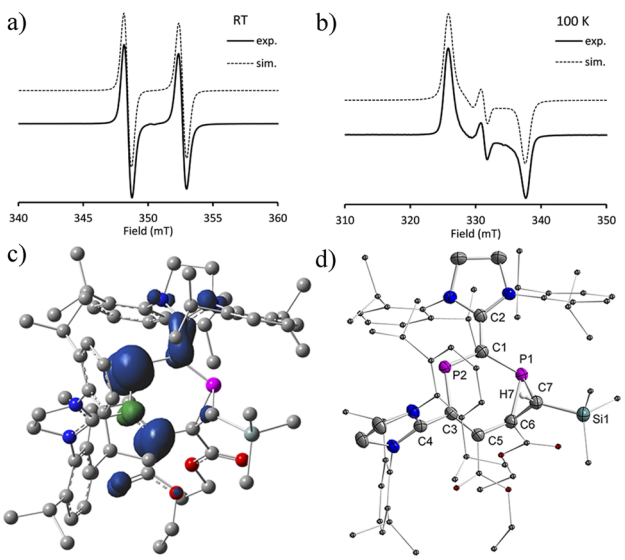

Fig. 9 a) Continuous wave EPR spectra at RT and (b) at 100 K; (c) spin density (density = 0.004) of $7^{\bullet+}$; (d) plots of the molecular structure of $7^{\bullet+}(BAr^{F})$ (ellipsoids are set to 50% probability; H atoms except H7 and anions are omitted for clarity). Selected distances (Å): $7^{\bullet+}$: P1–C1 1.743(2), P1–C6 1.867(2), P1–C7 1.848(2), C7–Si1 1.890(2), C7–C6 1.532(3), C6–C5 1.487(3), C5–C3 1.381(3), C3–P2 1.789(2), P2–C1 1.743(2), C1–C2 1.414(3), and C3–C4 1.498(3).

The structural metrics within the C2–C1–P2–C3–C4 unit (C2═C1 1.414(3) Å, P2–C1 1.743(2) Å, P2–C3 1.789(2) Å, and C3–C4 1.498(3) Å) indicate delocalization of both charge and spin density, which however only involves one phosphorus center. An NPA analysis shows that the majority of the spin density is delocalized over an allyl-type endocyclic P2–C3–C5 unit [spin density: P2 (0.39*e*), C3 (−0.07*e*), and C5 (0.31*e*)] with a very small contribution from C1 (0.08*e*) and virtually no spin density on P1 and C6 (Fig. 9c). The formation of $\mathbf{7}^{\bullet+}(BAr^F)$ further supports the presence of an allyl-type delocalized radical fragment in $\mathbf{2a,b}^{\bullet+}(BAr^F)$.

Conclusions

The octet rule predicts that CRCs only react with radical sites forming cations with eight valence electrons. In contrast, DRCs with spatially separated charge and radical sites are promising candidates to show both radical and cationic reactivity at different sites within one molecule. However, such dual reactivity has presently only been reported in the gas phase. In the condensed phase, a molecule with such dual reactivity has not been reported yet. In this work, delocalized DRCs $\mathbf{2a,b}^{\bullet+}(BAr^F)$ with an unsaturated radical and cationic site have been isolated and analysed by EPR spectroscopic analysis, XRD determination and DFT calculations. Indeed, $\mathbf{2a}^{\bullet+}(BAr^F)$, as an example, manifests sequential radical and cationic reactivity in the condensed phase. Attempts to demonstrate sequential cationic and radical reactivity of $\mathbf{2a,b}^{\bullet+}(BAr^F)$ failed, which may be attributed to the high instability of the resulting neutral radicals after reaction with a nucleophile. Furthermore, the reaction between $\mathbf{2a}^{\bullet+}(BAr^F)$ and azide anions indicates that the former may behave as a rather strong oxidant eventually generating transient azidyl radicals, which further complicates the chemistry of the DRCs reported here but also offers further applications in synthetic chemistry.

Data availability

All data associated with this article are available from ESI.†

Author contributions

S. Liu carried out most of the experimental work. J. Lin assisted with the HRMS measurements. Y. Li, Z. Ke, and Z. Li carried out the computational studies. The manuscript was written through contributions of all authors. All authors have given approval to the final version of the manuscript.

Conflicts of interest

There are no conflicts to declare.

Acknowledgements

This work was supported by the National Natural Science Foundation of China (22271315, 22171291, 21821003 and 21890380), Tip-top Scientific and Technical Innovative Youth Talents of Guangdong Special Support Program (2019TQ05C926), Guangdong Basic and Applied Basic Research Foundation (2021A1515012028 and 2023A1515010092), Science and Technology Planning Project of Guangzhou (202102080189) and National Key Research and Development Program of China (2021YFA1500401).

Notes and references

1 M. Gomberg, *J. Am. Chem. Soc.*, 1900, **22**, 757–771.
2 J. Thiele and H. Balhorn, *Ber. Dtsch. Chem. Ges.*, 1904, **37**, 1463–1470.
3 (*a*) C. D. Martin, S. Soleilhavoup and G. Bertrand, *Chem. Sci.*, 2013, **4**, 3020–3030; (*b*) Y. Su and R. Kinjo, *Coord. Chem. Rev.*, 2017, **352**, 346–378; (*c*) V. Nesterov, D. Reiter, P. Bag, P. Frisch, R. Holzner, A. Porzelt and S. Inoue, *Chem. Rev.*, 2018, **118**, 9678–9842; (*d*) L. L. Liu and D. W. Stephan, *Chem. Soc. Rev.*, 2019, **48**, 3454–3463; (*e*) Z. X. Chen, Y. Li and F. Huang, *Chem*, 2020, **7**, 1–45; (*f*) D. Wang, C. Zhai, Y. Chen, Y. He, X.-d. Chen, S. Wang, L. Zhao, G. Frenking, X. Wang and G. Tan, *Nat. Chem.*, 2023, **15**, 200–205; (*g*) Z. Feng, S. Tang, Y. Su and X. Wang, *Chem. Soc. Rev.*, 2022, **51**, 5930–5973; (*h*) K. Hatakeyama-Sato and K. Oyaizu, *Chem. Rev.*, 2023, **123**, 11336–11391; (*i*) M. Ju, Z. Lu, L. F. T. Novaes, J. I. Martinez Alvarado and S. Lin, *J. Am. Chem. Soc.*, 2023, **145**, 19478–19489; (*j*) I. Ratera and J. Veciana, *Chem. Soc. Rev.*, 2012, **41**, 303–349; (*k*) Z. X. Chen, Y. Li and F. Huang, *Chem*, 2021, **7**, 288–332; (*l*) J. E. Nutting, M. Rafiee and S. S. Stahl, *Chem. Rev.*, 2018, **118**, 4834–4885; (*m*) Y. K. Loh, P. Vasko, C. McManus, A. Heilmann, W. K. Myers and S. Aldridge, *Nat. Commun.*, 2021, **12**, 7052; (*n*) T. Ullrich, P. Pinter, J. Messelberger, P. Haines, R. Kaur, M. M. Hansmann, D. Munz and D. M. Guldi, *Angew. Chem., Int. Ed.*, 2020, **59**, 7906–7914.
4 (*a*) T. Li, H. Wei, Y. Fang, L. Wang, S. Chen, Z. Zhang, Y. Zhao, G. Tan and X. Wang, *Angew. Chem., Int. Ed.*, 2017, **56**, 632–636; (*b*) G. Tan and X. Wang, *Chin. J. Chem.*, 2018, **36**, 573–586; (*c*) Z. Feng, Y. Fang, H. Ruan, Y. Zhao, G. Tan and X. Wang, *Angew. Chem., Int. Ed.*, 2020, **59**, 6769–6774; (*d*) B. Wang, Y. Li, R. Ganguly, R. D. Webster and R. Kinjo, *Angew. Chem., Int. Ed.*, 2018, **57**, 7826–7829.
5 (*a*) B. F. Yates, W. J. Bouma and L. Radom, *J. Am. Chem. Soc.*, 1984, **106**, 5805–5808; (*b*) B. F. Yates, W. J. Bouma and L. Radom, *Tetrahedron*, 1986, **42**, 6225–6234.
6 (*a*) S. Hammerum, *Mass Spectrom. Rev.*, 1988, **7**, 123–202; (*b*) K. M. Stirk, L. K. M. Kiminkinen and H. I. Kenttamaa, *Chem. Rev.*, 1992, **92**, 1649–1665; (*c*) H. I. Kenttämaa, *Org. Mass Spectrom.*, 1994, **29**, 1–10; (*d*) D. M. Tomazela, A. A. Sabino, R. Sparrapan, F. C. Gozzo and M. N. Eberlin, *J. Am. Soc. Mass Spectrom.*, 2006, **17**, 1014–1022; (*e*) P. E. Williams, B. J. Jankiewicz, L. Yang and H. I. Kenttämaa, *Chem. Rev.*, 2013, **113**, 6949–6985.
7 (*a*) L. A. B. Moraes and M. N. Eberlin, *J. Am. Soc. Mass Spectrom.*, 2000, **11**, 697–704; (*b*) L. A. B. Moraes and M. N. Eberlin, *J. Am. Chem. Soc.*, 1998, **120**, 11136–11143.
8 (*a*) S. Tojo, S. Yasui, M. Fujitsuka and T. Majima, *J. Org. Chem.*, 2006, **71**, 8227–8232; (*b*) C. A. Marquez, H. Wang,

F. Fabbretti and J. O. Metzger, *J. Am. Chem. Soc.*, 2008, **130**, 17208–17209; (*c*) L. A. Rios, W. R. Dolbier, R. Paredes, J. Lusztyk, K. U. Ingold and M. Jonsson, *J. Am. Chem. Soc.*, 1996, **118**, 11313–11314; (*d*) F. Widjaja, Z. Jin, J. J. Nash and H. I. Kenttämaa, *J. Am. Chem. Soc.*, 2012, **134**, 2085–2093; (*e*) B. B. Noble and M. L. Coote, *J. Polym. Sci.*, 2020, **58**, 52–61; (*f*) M. L. Grimm, N. K. Suleman, A. N. Hancock, J. N. Spencer, T. Dudding, R. Rowshanpour, N. Castagnoli and J. M. Tanko, *J. Am. Chem. Soc.*, 2020, **142**, 2640–2652; (*g*) J. H. Horner and M. Newcomb, *J. Org. Chem.*, 2007, **72**, 1609–1616.

9 (*a*) R. P. Kohin and P. G. Nadeau, *J. Chem. Phys.*, 1966, **44**, 691–694; (*b*) E. A. C. Lucken and C. Mazeline, *J. Chem. Soc. A*, 1966, 1074–1077; (*c*) J. Sinclair, *J. Chem. Phys.*, 1971, **55**, 245–251; (*d*) L. Bonazzola, C. Iacona, J. P. Michaut and J. Roncin, *J. Chem. Phys.*, 1980, **73**, 4175–4177; (*e*) I. Janovský, W. Knolle, S. Naumov and F. Williams, *Chem.–Eur. J.*, 2004, **10**, 5524–5534.

10 (*a*) O. Back, M. A. Celik, G. Frenking, M. Melaimi, B. Donnadieu and G. Bertrand, *J. Am. Chem. Soc.*, 2010, **132**, 10262–10263; (*b*) X. Pan, X. Wang, Z. Zhang and X. Wang, *Dalton Trans.*, 2015, **44**, 15099–15102; (*c*) N. M. Gallagher, H. Z. Ye, S. Feng, J. Lopez, Y. G. Zhu, T. Van Voorhis, Y. Shao-Horn and J. A. Johnson, *Angew. Chem., Int. Ed.*, 2020, **59**, 3952–3955; (*d*) F. Biaso, T. Cantat, N. Mézailles, L. Ricard, P. Le Floch and M. Geoffroy, *Angew. Chem., Int. Ed.*, 2006, **45**, 7036–7039; (*e*) M. K. Sharma, S. Chabbra, C. Wolper, H. M. Weinert, E. J. Reijerse, A. Schnegg and S. Schulz, *Chem. Sci.*, 2022, **13**, 12643–12650; (*f*) X. Chen, L. L. Liu, S. Liu, H. Grützmacher and Z. Li, *Angew. Chem., Int. Ed.*, 2020, **59**, 23830–23835; (*g*) R. J. Andrews and D. W. Stephan, *Chem.–Eur. J.*, 2020, **26**, 7194–7198.

11 (*a*) C.-X. Miao, J.-Q. Wang, B. Yu, W.-G. Cheng, J. Sun, S. Chanfreau, L.-N. He and S.-J. Zhang, *Chem. Commun.*, 2011, **47**, 2697; (*b*) Y. Liu, M.-A. Goulet, L. Tong, Y. Liu, Y. Ji, L. Wu, R. G. Gordon, M. J. Aziz, Z. Yang and T. Xu, *Chem*, 2019, **5**, 1861–1870; (*c*) B. Rahman, K.-i. Kanbara, H. Akutsu, J.-i. Yamada and S. i. Nakatsuji, *Polyhedron*, 2007, **26**, 2287–2290; (*d*) S. Aonuma, H. Casellas, C. Faulmann, B. Garreau de Bonneval, I. Malfant, P. Cassoux, P. G. Lacroix, Y. Hosokoshi and K. Inoue, *J. Mater. Chem.*, 2001, **11**, 337–345; (*e*) T. Hirashita, M. Nakanishi, T. Uchida, M. Yamamoto, S. Araki, I. W. C. E. Arends and R. A. Sheldon, *ChemCatChem*, 2016, **8**, 2704–2709; (*f*) N. Jayaraj, M. Porel, M. F. Ottaviani, M. V. S. N. Maddipatla, A. Modelli, J. P. Da Silva, B. R. Bhogala, B. Captain, S. Jockusch, N. J. Turro and V. Ramamurthy, *Langmuir*, 2009, **25**, 13820–13832.

12 (*a*) T. Weiske, H. V. D. Wel, N. M. M. Nibbering and H. Schwarz, *Angew. Chem.*, 1984, **96**, 694–695; (*b*) P. Mourgues, H. E. Audier, D. Leblanc and S. Hammerum, *Org. Mass Spectrom.*, 1993, **28**, 1098–1100; (*c*) A. E. P. M. Sorrilha, F. C. Gozzo, R. S. Pimpim and M. N. Eberlincor, *J. Am. Soc. Mass Spectrom.*, 1996, **7**, 1126–1137.

13 Z. Li, X. Chen, D. M. Andrada, G. Frenking, Z. Benkö, Y. Li, J. R. Harmer, C.-Y. Su and H. Grützmacher, *Angew. Chem., Int. Ed.*, 2017, **56**, 5744–5749.

14 P. Coburger, C. Schweinzer, Z. Li and H. Grützmacher, *Angew. Chem., Int. Ed.*, 2023, **62**, e202214548.

15 Z. Li, Y. Hou, Y. Li, A. Hinz and X. Chen, *Chem.–Eur. J.*, 2018, **24**, 4849–4855.

16 (*a*) A. Hinz, A. Schulz, W. W. Seidel and A. Villinger, *Inorg. Chem.*, 2014, **53**, 11682–11690; (*b*) L. Chojetzki, A. Schulz, A. Villinger and R. Wustrack, *Z. Anorg. Allg. Chem.*, 2020, **646**, 614–624; (*c*) T. Beweries, R. Kuzora, U. Rosenthal, A. Schulz and A. Villinger, *Angew. Chem., Int. Ed.*, 2011, **50**, 8974–8978.

17 (*a*) Z. Li, Y. Hou, Y. Li, A. Hinz, J. R. Harmer, C.-Y. Su, G. Bertrand and H. Grützmacher, *Angew. Chem., Int. Ed.*, 2018, **57**, 198–202; (*b*) X. Chen, A. Hinz, J. R. Harmer and Z. Li, *Dalton Trans.*, 2019, **48**, 2549–2553; (*c*) L. Liu, L. L. Cao, Y. Shao, G. Ménard and D. W. Stephan, *Chem*, 2017, **3**, 259–267; (*d*) A. Brückner, A. Hinz, J. B. Priebe, A. Schulz and A. Villinger, *Angew. Chem., Int. Ed.*, 2015, **54**, 7426–7430; (*e*) Y. Su, X. Zheng, X. Wang, X. Zhang, Y. Sui and X. Wang, *J. Am. Chem. Soc.*, 2014, **136**, 6251–6254; (*f*) X. Pan, Y. Su, X. Chen, Y. Zhao, Y. Li, J. Zuo and X. Wang, *J. Am. Chem. Soc.*, 2013, **135**, 5561–5564; (*g*) X. Pan, X. Chen, T. Li, Y. Li and X. Wang, *J. Am. Chem. Soc.*, 2013, **135**, 3414–3417; (*h*) G. Ménard, J. A. Hatnean, H. J. Cowley, A. J. Lough, J. M. Rawson and D. W. Stephan, *J. Am. Chem. Soc.*, 2013, **135**, 6446–6449; (*i*) S. Ishida, F. Hirakawa and T. Iwamoto, *J. Am. Chem. Soc.*, 2011, **133**, 12968–12971; (*j*) R. Kinjo, B. Donnadieu and G. Bertrand, *Angew. Chem., Int. Ed.*, 2010, **49**, 5930–5933; (*k*) O. Back, B. Donnadieu, P. Parameswaran, G. Frenking and G. Bertrand, *Nat. Chem.*, 2010, **2**, 369.

18 M. Melaimi, R. Jazzar, M. Soleilhavoup and G. Bertrand, *Angew. Chem., Int. Ed.*, 2017, **56**, 10046–10068.

19 (*a*) X. Zhang, X. Chen, H. Zhai, S. Liu, C. Hu, L. L. Liu, S. Wang and Z. Li, *Dalton Trans.*, 2020, **49**, 6384–6390; (*b*) X. Chen, C. Hu, X. Zhang, S. Liu, Y. Mei, G. Hu, L. L. Liu, Z. Li and C.-Y. Su, *Inorg. Chem.*, 2021, **60**, 5771–5778; (*c*) C. C. Chong, B. Rao, R. Ganguly, Y. Li and R. Kinjo, *Inorg. Chem.*, 2017, **56**, 8608–8614.

20 M. J. Frisch, *et al.*, *Gaussian 16*, Revision C.01, 2016.

21 E. D. Glendening, J. K. Badenhoop, A. E. Reed, J. E. Carpenter, J. A. Bohmann, C. M. Morales, P. Karafiloglou, C. R. Landis and F. Weinhold, *NBO 7.0*, 2018.

22 (*a*) M.-L. Y. Riu, A. K. Eckhardt and C. C. Cummins, *J. Am. Chem. Soc.*, 2022, **144**, 7578–7582; (*b*) C. Jones and M. Waugh, *Dalton Trans.*, 2004, 1971–1979; (*c*) L. E. Longobardi, C. A. Russell, M. Green, N. S. Townsend, K. Wang, A. J. Holmes, S. B. Duckett, J. E. McGrady and D. W. Stephan, *J. Am. Chem. Soc.*, 2014, **136**, 13453–13457; (*d*) S. Wang, K. Samedov, S. C. Serin and D. P. Gates, *Eur. J. Inorg. Chem.*, 2016, **2016**, 4144–4151.

23 (*a*) P. Pyykkö and M. Atsumi, *Chem.–Eur. J.*, 2009, **15**, 12770–12779; (*b*) F. H. Allen, O. Kennard, D. G. Watson, L. Brammer, A. G. Orpen and R. Taylor, *J. Chem. Soc., Perkin Trans. 2*, 1987, **2**, S1–S19.

24 (*a*) T. Völzer, H. Beer, A. Schulz, S. Lochbrunner and J. Bresien, *Phys. Chem. Chem. Phys.*, 2021, **23**, 7434–7441; (*b*) H. Beer, J. Bresien, D. Michalik, A. Schulz and A. Villinger, *Dalton Trans.*, 2020, **49**, 13986–13992; (*c*) J. Bresien, T. Kröger-Badge, S. Lochbrunner, D. Michalik, H. Müller, A. Schulz and E. Zander, *Chem. Sci.*, 2019, **10**, 3486–3493; (*d*) A. Hinz, A. Schulz and A. Villinger, *Angew. Chem., Int. Ed.*, 2015, **54**, 2776–2779; (*e*) A. Hinz, A. Schulz and A. Villinger, *J. Am. Chem. Soc.*, 2015, **137**, 9953–9962.

25 Z.-Y. Wang, Y.-Z. Dai, L. Ding, B.-W. Dong, S.-D. Jiang, J.-Y. Wang and J. Pei, *Angew. Chem., Int. Ed.*, 2021, **60**, 4594–4598.

26 P. Agarwal, N. A. Piro, K. Meyer, P. Müller and C. C. Cummins, *Angew. Chem., Int. Ed.*, 2007, **46**, 3111–3114.

27 (*a*) N. Fu, G. S. Sauer, A. Saha, A. Loo and S. Lin, *Science*, 2017, **357**, 575–579; (*b*) H. M. Nelson, J. C. Siu, A. Saha, D. Cascio, S. N. MacMillan, S.-B. Wu, C. Lu, J. A. Rodríguez, K. N. Houk and S. Lin, *Org. Lett.*, 2021, **23**, 454–458; (*c*) J. C. Siu, G. S. Sauer, A. Saha, R. L. Macey, N. Fu, T. Chauviré, K. M. Lancaster and S. Lin, *J. Am. Chem. Soc.*, 2018, **140**, 12511–12520.